Composition of KBO (50000) Quaoar

Cristina M. Dalle Ore, Maria Antonella Barucci, Joshua P. Emery, Dale P. Cruikshank, L. V. Dalle Ore, Frédéric Merlin, Alvaro Alvarez-Candal, Catherine de Bergh, David E. Trilling, Davide Perna, et al.

A&A 501, 349–357 (2009)
DOI: 10.1051/0004-6361/200911752

Astronomy & Astrophysics

Composition of KBO (50000) Quaoar⋆

C. Morea Dalle Ore[1,3], M. A. Barucci[2], J. P. Emery[4], D. P. Cruikshank[1], L. V. Dalle Ore[1], F. Merlin[5], A. Alvarez-Candal[2], C. de Bergh[2], D. E. Trilling[8], D. Perna[2,6,7], S. Fornasier[2], R. M. E. Mastrapa[1,3], and E. Dotto[6]

[1] NASA Ames Research Center, Mail Stop 245-6, Moffett Field, CA 94035, USA
e-mail: [Cristina.M.DalleOre;Dale.P.Cruikshank;Rachel.M.Mastrapa]@nasa.gov
[2] LESIA, Observatoire de Paris, 92195 Meudon Pricipal Cedex, France
e-mail: [Antonella.Barucci;Catherine.deBergh;Sonia.Fornasier;Alvaro.Alvarez;Davide.Perna]@obspm.fr
[3] SETI Institute, 515 N. Whisman Rd., Mountain View, CA 94043 CA, USA
[4] Earth and Planetary Sciences Dept, University of Tennessee, Knoxville, TN 37996, USA
e-mail: JEmery2@utk.edu
[5] Department of Astronomy, University of Maryland, College Park, MD 20742, USA
e-mail: Frederic.Merlin@obspm.fr
[6] INAF, Osservatorio Astronomico di Roma, via Frascati 33, 00040 Monteporzio Catone, Roma, Italy
e-mail: Dotto@mporzio.astro.it
[7] Università di Roma Tor Vergata, via della Ricerca Scientifica 1, 00133 Roma, Italy
[8] Department of Physics and Astronomy, Northern Arizona University, Flagstaff, AZ 86011, USA
e-mail: David.Trilling@nau.edu

Received 30 January 2009 / Accepted 7 April 2009

ABSTRACT

Aims. The objective of this work is to investigate the physical properties of objects beyond Neptune – the new frontiers of the Solar System – and in particular to study the surface composition of (50 000) Quaoar, a classical Transneptunian (or Kuiper Belt) object. Because of its distance from the Sun, Quaoar is expected to have preserved, to a degree, its original composition. Our goals are to determine to what degree this is true and to shed light on the chemical evolution of this icy body.
Methods. We present new near-infrared (3.6 and 4.5 μm) photometric data obtained with the *Spitzer Space Telescope*. These data complement high resolution, low signal-to-noise spectroscopic and photometric data obtained in the visible and near-infrared (0.4–2.3 μm) at VLT-ESO and provide an excellent set of constraints in the model calculation process. We perform spectral modeling of the entire wavelength range – from 0.3 to 4.5 μm by means of a code based on the Shkuratov radiative transfer formulation of the slab model. We also attempt to determine the temperature of H_2O ice making use of the crystalline feature at 1.65 μm.
Results. We present a model confirming previous results regarding the presence of crystalline H_2O and CH_4 ice, as well as C_2H_6 and organic materials, on the surface of this distant icy body. We attempt a measurement of the temperature and find that stronger constraints on the composition are needed to obtain a precise determination.
Conclusions. Model fits indicate that N_2 may be a significant component, along with a component that is bright at $\lambda > 3.3$ μm, which we suggest at this time could be amorphous H_2O ice in tiny grains or thin grain coatings. Irradiated crystalline H_2O could be the source of small-grained amorphous H_2O ice. The albedo and composition of Quaoar, in particular the presence of N_2, if confirmed, make this TNO quite similar to Triton and Pluto.

Key words. techniques: spectroscopic – Kuiper Belt

1. Introduction

(50 000) Quaoar, discovered in 2002, is a classical Transneptunian (or Kuiper Belt) object. It orbits the Sun with a nearly circular orbit ($e = 0.039$) that has a rather low inclination to the ecliptic ($i = 8°$). Its semi-major axis is at 43.574 AU ($q = 41.872$ AU; $Q = 45.275$ AU).

Quaoar is one of the largest Transneptunian objects ever discovered. First estimates of its diameter were based on direct size measurements with the Hubble Space Telescope by Brown & Trujillo (2004), who found its diameter to be 1260 ± 190 km. More recent data using thermal infrared photometric measurements with the *Spitzer Space Telescope* have led to an estimated diameter of 840 (+200, –190) km (Stansberry et al. 2008).

The surface of Quaoar is intermediate in albedo with respect to other TNOs, with a visible geometric albedo of about 0.2 (Stansberry et al. 2008). In addition, it has been found that Quaoar is a very red object (spectral slope in the visible: around 28% per 100 nm; Marchi et al. 2003; Alvarez-Candal et al. 2008; Fornasier et al. 2004) and has been classified as an RR object in the Barucci taxonomic system (DeMeo et al. 2009). The *R*-band polarimetric observations of Quaoar for solar phase angles in the 0.25–1.23 degree range indicate a nearly constant, relatively weak negative polarization (Bagnulo et al. 2006). As discussed by Bagnulo et al. (2008), this polarimetric behavior resembles more that of Eris and Pluto than of smaller objects. Photometric observations in the *R* band carried out at the same time by Bagnulo et al. (2006) show a linear phase curve. Rabinowitz et al. (2007) have published a more complete study of the phase curve of Quaoar with measurements in the *B*, *V* and *I* bands, and more data points in each band, and show that the phase

⋆ Based on observations at the VLT Observatory Cerro Paranal of European Southern Observatory, ESO, Chile, in the framework of program 178.C-0036.

curve is significantly wavelength dependent. The rotation period of Quaoar is approximately 17.68 h, showing a double-peaked lightcurve (Ortiz et al. 2003). Quaoar has one known satellite (at about 0.35″ from Quaoar at discovery) with brightness in R about 6 mag fainter than the primary (Brown & Suer 2007).

The first spectroscopic observations of Quaoar were made in the visible range using the ESO-NNT (Marchi et al. 2003). They did not reveal any spectral bands, only a very red spectral slope. The first near-IR spectroscopic observations of Quaoar were obtained with the Subaru telescope (Jewitt & Luu 2004). They showed very clearly the presence of crystalline H_2O ice at the surface of this large TNO. There was also an indication of a very weak absorption band at 2.2 μm, with similarities to that observed on Charon at the same wavelength. The band on Quaoar was tentatively assigned to ammonia hydrate (as for Charon). To explain the presence of crystalline H_2O ice and possibly of ammonia hydrate on the surface of this body, Jewitt & Luu (2004) concluded that resurfacing mechanisms must exist on Quaoar, probably indicating cryovolcanism. We also note that Cook et al. (2007), who retrieved several unpublished spectra of Quaoar obtained at the Subaru telescope at different times, found that the band at 2.2 μm, although always present, does not always appear at the same wavelength position. They proposed the presence of different hydration states for the ammonia hydrate, varying with surface location.

More recent observations by Schaller & Brown (2007b) with the Keck telescope confirmed the presence of a weak band at 2.2 μm, but it was instead assigned to CH_4 ice, as CH_4 also fits stronger absorption bands at longer wavelengths (around 2.32 and 2.38 μm). Furthermore, slight remaining differences between the observed spectra and modeled spectra that included H_2O ice and CH_4 ice were best explained by the presence of ethane, another hydrocarbon ice, that is a likely by-product of CH_4 irradiation (Baratta et al. 2003). The detection of small amounts of CH_4 on Quaoar is not too surprising. Indeed, Schaller & Brown (2007a) have shown that, given its size and distance from the Sun, Quaoar could have retained at least some of the very volatile species like CH_4, N_2 or CO that are observed on the surface of Pluto and other TNOs larger than Quaoar.

In the course of a Large Programme at ESO-VLT (P.I. M.A. Barucci) we have obtained for this KBO visible and near-infrared photometry (DeMeo et al. 2009) and nearly simultaneous spectra in the visible (from 0.4 to 0.85 μm) and near-IR (J, H, and K bands). In this paper we have combined the visible (Alvarez-Cantal et al. 2008) and SINFONI $H + K$ spectrum (Guilbert et al. 2009) with a J spectrum obtained the same night at ESO-VLT with the ISAAC instrument, as well as with broad-band photometric data at 3.6 and 4.5 μm obtained at a different time with the *Spitzer Space Telescope*. Based on this extended set of data, we present a new interpretation of the surface composition of Quaoar.

2. Observational data

The data reported herein are a combination of spectroscopic and photometric data obtained in the visible and near-infrared (0.4–2.3 μm) at VLT-ESO (Cerro Paranal, Chile) in conjunction with photometric data at 3.6 and 4.5 μm from the *Spitzer Space Telescope*. Table 1 illustrates the observing circumstances for Quaoar.

2.1. VLT-ESO data

The VLT data were collected during the night of 15 July 2007 in service mode using three different instruments: FORS1, visible photometry and spectroscopy; ISAAC, $J - H - K_s$ photometry and J spectroscopy; and SINFONI $H + K$ spectroscopy. All three instruments were working simultaneously at UT1, UT2 and UT4 telescopes at Cerro Paranal (ESO, Chile).

2.1.1. Spectroscopy

The visible observations, covering the 0.4–0.94 μm wavelength range, were acquired by Alvarez-Candal et al. (2008) with a spectral resolution of about 200. All the details of observations and reduction strategies are reported in Alvarez-Candal et al. (2008).

J-band spectroscopy in the range 1.1–1.4 μm, presented here for the first time, was performed using ISAAC in the short wavelength mode with a spectral resolution of about 500. The object was nodded between positions A and B along the 1″ wide slit for a total exposure time of 20 min (10 exposures of DIT = 120 s). The A and B images, taken 10″ apart, were subtracted and combined using MIDAS following the procedure described by Barucci et al. (2002). The reflectance spectrum of the target object was obtained by dividing the spectrum of the observed object by the spectrum of the solar analog HD 147284 observed at airmass within a few percent from that of Quaoar. This J spectrum was smoothed using a median filter to reach a spectral resolution of about 100, in order to improve the signal-to-noise ratio.

The H- and K-band spectroscopy (Guilbert et al. 2009) was obtained using SINFONI, a near-infrared integral field spectrometer, installed on UT4-"Yepun" ESO-VLT. For these observations the $H + K$ grating was used yielding a spectral resolution of about 1500 over the 1.45–2.45 μm range. A median filtering technique was applied in order to remove bad pixels and residual spikes. See Guilbert et al. (2009) for all details on observations and data reduction. The spectrum was smoothed to a resolution of about 250.

Since different spectral ranges were covered with different instruments and setups, we adjusted the flux scale of each spectrum using the photometric colors obtained almost-simultaneously (DeMeo et al. 2009) and listed in Table 2.

2.1.2. Combining the data

To combine the different spectral ranges we use the photometric data reported in Table 2. First we normalize to unity the visible spectra at the effective wavelength of the V filter. Then we rescale the R, J, H, and K colors (Table 2) using

$$R_{\lambda_e} = 10^{-0.4[(M_{\lambda_e}-V)-(M_{\lambda_e}-V)_\odot]}$$

where $(M_{\lambda_e} - V)$ and $(M_{\lambda_e} - V)_\odot$ are the colors of Quaoar and the Sun, respectively (see Delsanti et al. 2004), and λ_e is the effective wavelength of the filter used to measure M_{λ_e}.

The obtained reflectances R_{λ_e} are used to re-normalize the other spectral ranges by means of a weighted mean, where the weights are given by the different transmission channels of the ISAAC filters J, H and K_s (T_λ). The re-normalized spectrum is then given by

$$F^n_\lambda = \left[\left(\frac{\sum_i T_i F_i}{\sum_i T_i}\right)^{-1} R_{\lambda_e}\right] F_\lambda$$

Table 1. Observing circumstances of (50000) Quaoar.

Observation	Date	Time (UT)	λ range (μm)	Spectral Res.	Integ. time (s)	Calib. Star
FORS1	15 July 07	01:56–02:36	0.4–0.94	200	2400	HD 147284
ISAAC	15 July 07	03:07–03:27	1.1–1.4	500	1200	HD 147284
SINFONI	15 July 07	01:54–03:34	1.45–2.45	1500 (250)	6000	HD 147935
VR Phot.	15 July 07	01:33–01:33	VR	–	40	–
JHK Phot.	15 July 07	02:17–02:22	JHK_s	–	300	–
IRAC	15 Sep. 07	01:12–02:10	3.6 & 4.5	5.2	1600	–
	18 Sep. 07	07:17–08:15	3.6 & 4.5	5.2	1600	–

Table 2. Photometric observations of (50 000) Quaoar from DeMeo et al. (2009).

Color	Magnitude (error)	Instrument
V	19.25 (0.05)	FORS1
$V-R$	0.60 (0.05)	FORS1
$V-J$	2.18 (0.06)	ISAAC
$V-H$	2.54 (0.06)	ISAAC
$V-K_s$	2.57 (0.06)	ISAAC

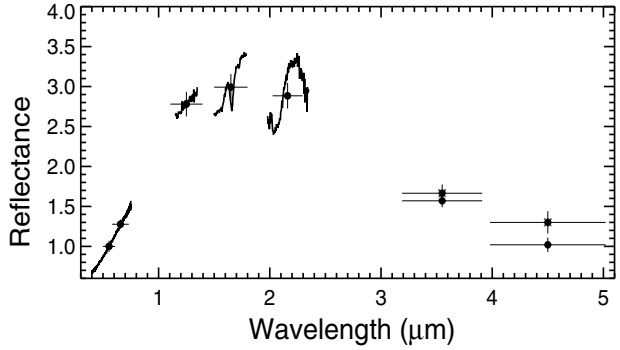

Fig. 1. Datasets adopted in the modeling process. The reflectance was normalized to 1.0 at 0.55 μm. The horizontal bars for each data point indicate the width of the filter band.

where F_λ is the original spectrum. The final spectrum is shown in Fig. 1 along with the other observations adopted in this paper. Based on measurements of the point to point scatter in the spectral region around 2.2 μm, a representative sample of average quality data, we estimate the noise to vary between 3% and 6%.

2.2. Spitzer *data*

The ground-based reflectance data have been complemented and extended to longer wavelengths with broadband photometric measurements from the InfraRed Array Camera (IRAC) on the *Spitzer Space Telescope* (Werner et al. 2004; Fazio et al. 2004). Two observations separated by 3.25 days (4.4 rotations for 17.6788 h period) each detected Quaoar at both 3.6 and 4.5 μm ($FWHM \simeq 0.68$ and 0.87 μm, respectively). Between the two dates, Quaoar moved $\simeq 1'$ within the 5.2′ FOV of IRAC, enabling accurate subtraction of background flux. Each observation consisted of a 16 point dither pattern of 100 s frames for the 4.5 μm channel followed immediately by a 16 point dither pattern of 100 s frames for the 3.6 μm channel. During the original cryogenic mission, IRAC imaged the same FOV at 5.8 μm simultaneously with the 3.6 μm channel and at 8.0 μm simultaneously with the 4.5 μm channel. Quaoar was not detected in either of the two longer wavelength channels.

The images have all been processed with the IRAC automated data pipeline (version 14.0), which includes steps such as dark subtraction, flat fielding, and flux calibration (see data handbook at ssc.spitzer.caltech.edu/irac/dh/). We average the 16 calibrated frames from each observation (omitting outliers) to calculate a background frame for the other date. This background frame is subtracted from each data frame and corrections (supplied by the *Spitzer Science Center*) for variation in pixel solid angle and array location dependent photometric variations are applied. Aperture photometry is performed using 2 and 3 pixel radius apertures and aperture corrections published in the IRAC data handbook. We calculate color corrections assuming a solar spectral slope through the IRAC channels (Smith & Gottlieb 1974). Final fluxes are the average of all sixteen frames (omitting outliers), and the 1-sigma uncertainties take into account photon counting statistics, variation among the 16 dithered frames, and variation among the different aperture measurements (Table 3). We also list magnitudes calculated from the measured fluxes using zero magnitude fluxes derived from data in Reach et al. (2005) (and posted at http://ssc.spitzer.caltech.edu/irac/calib/). The geometric albedo in each channel is calculated from

$$p_\lambda = \frac{F_\lambda r_{\rm AU}^2 \Delta^2}{F_{\lambda\odot} \Phi R^2}$$

where F_λ is the measured flux, $r_{\rm AU}$ is the heliocentric distance in AU, Δ is the geocentric distance, $F_{\lambda\odot}$ is the solar flux at 1 AU, Φ is a phase correction, and R is the object's radius. Rabinowitz et al. (2007) report a linear phase coefficient for Quaoar that differs significantly in the B, V, and I filters. They attribute this to an albedo dependence of the coherent backscatter opposition effect. The IRAC albedos fall between the V and I albedos, so we iteratively do a linear interpolation in phase coefficient-albedo space to estimate the phase coefficient for the IRAC measurements. We use the radius of Quaoar reported by Stansberry et al. (2008) from *Spitzer* thermal emission measurements (R = 422 km, p_v = 0.199). As long as the 0.4 to 2.5 μm spectrum is scaled to the p_v that is consistent with the size used in the IRAC albedo calculation, the relative spectral albedos between the ground-based and IRAC data should be correct. The relationship between R and p_v is set by the absolute magnitude (H_v), which has been well-measured for Quaoar, including corrections for phase function and light curve (2.729 ± 0.025; Rabinowitz et al. 2007; Bagnulo et al. 2006).

We use the measured light curve (Ortiz et al. 2003; Rabinowitz et al. 2007) to calculate the rotational phases of the various observations used herein. Thirouin et al. (2009, in preparation) have reanalyzed the data of Ortiz et al. (2003), confirming the rotation period of 17.6788 ± 0.0004 h (J. Ortiz, personal communication). We find that the Spitzer thermal (MIPS) observations used by Stansberry et al. (2008) to estimate the size of Quaoar are perfectly phased with the ground-based data

Table 3. Measured fluxes and albedos from IRAC.

		Original				Lighcurve Corrected				
Date	λ (μm)	Flux (μJy)	ΔFlux (μJy)	mag	Δmag	Flux (μJy)	ΔFlux (μJy)	p^a_λ	Δp_λ	Phase Coef. (mag/deg)
15 Sep. 2005	3.6	28.00	1.28	17.50	±0.05	26.76	1.54	0.290	0.018	0.252
	4.5	14.06	1.26	17.77	±0.10	13.44	1.29	0.192	0.019	0.136
18 Sep. 2005	3.6	28.78	1.74	17.47	±0.07	29.14	2.10	0.341	0.026	0.313
	4.5	16.46	1.75	17.60	±0.12	16.67	1.89	0.266	0.031	0.224

[a] Geometric albedo. Assumes R = 422 km (consistent with p_v = 0.199).

(within ±9° in longitude). The first IRAC date falls ~30° in longitude away (falling on the brightest part of the light curve), whereas the second IRAC date is nearly perfectly 180° away from the ground-based/MIPS rotational phase. Using this information, we corrected the measured IRAC fluxes to the rotational phase of the ground-based and MIPS observations. Lightcurve-corrected IRAC albedos were then rederived as outlined above. Uncertainties in brightness from propagating the rotational phase have been folded into the final albedo uncertainties. While the best lightcurve solution predicts a double-peaked lightcurve (with one maximum ~0.02 mag brighter than the other), there is a small chance that the lightcurve is single-peaked. In this case, the second IRAC date would fall on the same rotational phase as the ground-based and MIPS observations, and the first IRAC data would be ~30° away.

3. Data analysis

3.1. Initial constraints and modeling strategy

The best and most straightforward way to identify surface materials spectroscopically is by detection of diagnostic absorption bands. Constraints on the presence of other materials necessarily rely on more subtle effects on the spectrum. With a spectrum as rich as that of Quaoar, we can be quite confident of the presence of several materials and have a good idea of others to consider prior to beginning the spectral modeling.

H_2O is clearly present as indicated by its distinctive bands at 1.5 and 2.0 μm (Jewitt & Luu 2004; Schaller & Brown 2007b). Furthermore, the distinctive 1.65 μm feature reveals that at least a significant portion of the H_2O is in the crystalline phase. This feature also provides a tool to determine the temperature of the ice on the surface of Quaoar. Several smaller absorption features (at 1.72, 2.32, and 2.38 μm) point strongly to the presence of CH_4 ice, as described by Schaller & Brown (2007b).

Several other materials are also hinted at, though less securely than H_2O and CH_4. The steep red slope from the visible through ≃1.3 μm is strongly suggestive of complex organic material. No other plausible material has yet been identified that can explain such steep spectral slopes (Cruikshank et al. 2005, and references therein). The slight difference in albedo at the second IRAC band (4.6 μm) between the two observations is suggestive of a possible variation in composition. The fact that the variation is present mostly in the second band is a constraint to the identification of the material that might be varying. Schaller & Brown (2007b) have reported the possible presence of ethane or other light hydrocarbons on the basis of weak features visible between 2.3 and 2.35 μm, and Jewitt & Luu (2004) suggested the presence of NH_4OH to explain a weak 2.2 μm feature. The goal of the present work is to test, via reflectance spectral modeling, which of the aforementioned materials are indeed present on the surface of Quaoar and to establish the relative amounts of the main components contributing to the spectral albedo. To achieve this goal we compile a list of candidate components and test in a quantitative way which materials affect the spectrum significantly in terms of feature matching, continuum level and overall fit.

3.2. Albedo determination

The overall albedo of a spectrum is an important constraint in developing spectral models. This is particularly important when considering components that lack discrete absorption features in the wavelength range being studied. According to Stansberry et al. (2008) Quaoar is a fairly bright object with visual albedo of 19.9% (+13.17%–7.04%) determined by *Spitzer/MIPS* measurements of thermal emission from Quaoar at 24 and 70 μm. We have therefore scaled the combined spectrum to the visible geometric albedo measured by Stansberry et al. (2008) before computing spectral models.

3.3. Modeling

3.3.1. Adopted code

The geometric albedo of Quaoar at every wavelength is calculated by means of a code based on the Shkuratov (1999) radiative transfer formulation of the slab model. Shkuratov differs from Hapke's (1981) approach in the treatment of the phase function (which is calculated rather than assigned as an explicit parameter as in Hapke) (see Poulet et al 2002, for a comparison of the theories) as well as in the number of free input parameters. Shkuratov's formulation, as well as Hapke's, allows mixing of materials in a variety of ways that include molecular as well as intimate mixtures. Molecular mixtures consist of inclusions in a medium (usually ice) of contaminant particles. In this case, optical constants for the contaminated material are calculated by means of the effective medium theory (Shkuratov 1999). Intimate mixtures are the common salt and pepper mixtures.

Required input parameters are the relative amounts, grain size and optical constants of the selected components. In the case of Quaoar, the fact that the adopted wavelength range is quite extensive increases the number of constraints and contributes to limiting the number of multiple solutions.

Optical constants (real and imaginary indices of refraction, covering the same wavelengths as the observations), are available for only a limited number of materials and can be a limiting factor when modeling the surface of Quaoar and other Solar System bodies. The determination of optical constants from laboratory spectral data is often challenging and can result in substantial uncertainties, particularly in regions of the spectrum

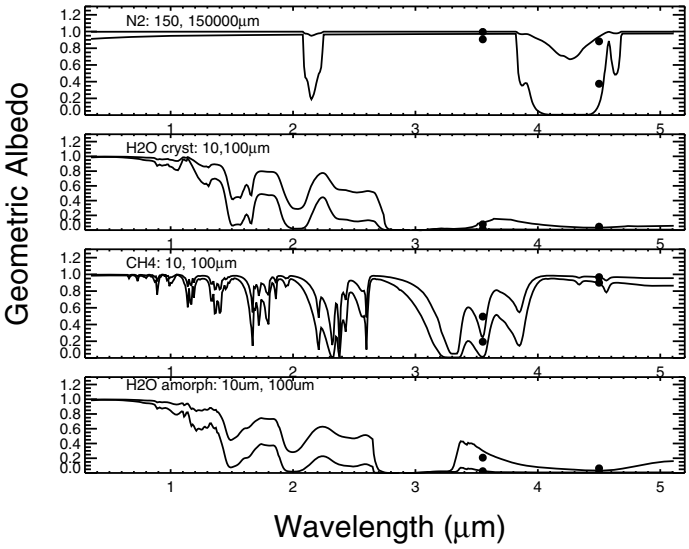

Fig. 2. Geometric albedo of ices calculated with Shkuratov's method for different grain sizes (smaller grains produce shallower lines). Dots at the *Spitzer* wavelengths correspond to the position of "synthetic *Spitzer* bands" calculated integrating the models over the *Spitzer* filters wavelength ranges. The N_2 spectrum represents the hexagonal β-phase, which is stable for $T \geq 35.6$ K. The analogous absorption bands for the cubic α-phase (stable for $T < 36$ K) are narrower.

where absorption is very weak (Mastrapa et al. 2008). Table 4 lists the materials that we adopted for the modeling of Quaoar and the sources of the optical constants. We refer to each individual paper for an assessment of the uncertainty in the optical constants of each component.

3.3.2. Impact of individual materials on the spectrum

Each selected component plays an important role in the overall spectrum or parts of it. In some cases, such as for H_2O, the effect is obvious and consists of the presence of discrete absorption bands, in others either the fundamental spectral bands fall outside the observed spectral range or the material has a featureless spectrum. In the latter case, the effect on the whole spectrum or on large parts of it can be quite subtle.

Many of the materials that are likely to exist on KBO surfaces have stronger absorptions in the 3 to 5 μm range than at shorter wavelengths, as shown in Fig. 2. This has also been observed on the surfaces of Pluto and Charon (Olkin et al. 2007; and Protopapa et al. 2008), even though, unlike the Quaoar case, on Pluto the 3.6 μm band is significantly lower than the 4.5 μm band. The *Spitzer* measurements are aimed at searching for these strong absorptions.

When CH_4, for example, is predominant in the mixture its effect is recognizable not only at 2.3 μm where its bands can be detected, but also at the *Spitzer* wavelengths: the first IRAC band will be lower than the second because of the significant absorption at 3.3 μm (see Fig. 2). N_2 on the other hand, is almost featureless in the visible and near-IR part of the spectrum, with the exception of its relatively weak band at 2.15 μm. The stronger band of N_2 at 4.3 μm can lower the second IRAC band (4.5 μm) relative to the first (3.6 μm). In the case of Quaoar, N_2 could be either in its cubic α-phase (stable for $T < 36$ K) or in its hexagonal β-phase, which is stable for $T \geq 35.6$ K, introducing bands of different strength and possibly affecting the IRAC bands a different amount.

Crystalline H_2O ice is extremely absorbing at the *Spitzer* wavelengths darkening the albedo significantly, but amorphous H_2O ice is less absorbing at 3.6 μm, setting it apart from its symmetrical counterpart. Triton tholin, a complex organic material, brightens the albedo at the *Spitzer* wavelengths and imparts a significant red slope in the visual part of the spectrum. Some minerals, such as pyroxenes, also have a relatively high albedo in the IR part of the spectrum.

When these spectral behaviors of ices and Quaoar constraints are kept into account the outline of a set of materials that are likely to play an important role starts taking shape. In the case of Quaoar we find that the main contributors to the overall albedo and shape of the spectrum are CH_4, N_2, and H_2O mixed intimately with tholins. The modeling of the red slope in the visible part of the spectrum indicates that CH_4 and H_2O ice are also mixed molecularly with tholins.

A few further materials were tested, at different stages of the modeling process, to determine whether a better fit could be achieved, particularly in the mid-IR part of the spectrum. These materials include minerals (olivine, pyroxene, NaCl) as well as alternative reddening materials (polyHCN) and ices (NH_3). They were originally chosen as they are fairly bright in the region of the Spitzer bands or because, in the case of NH_3, we were testing for irradiation products of CH_4 and N_2 (Moore & Hudson 2003; Piscitelli et al. 1988). They were ultimately abandoned in favor of the components that are part of the final model as their behavior did not reflect the observation requirements. NaCl was the only one that provided as good a fit as the H_2O in very small grains, but wasn't adopted as the very limited inventory of Cl in the Solar System makes it an unlikely candidate.

Grain sizes were initially estimated based on the strength of the visible features, for those materials such as CH_4 and H_2O, that have bands in the observed wavelength range. The grain sizes of the components whose bands are not observable were estimated to be comparable in size to the grains of the components with observed bands. N_2 is the exception as this ice requires very long path lengths to produce detectable absorptions, and our initial guess reflected commonly detected grain sizes for it.

The list of candidate materials, tentative grain sizes and relative amounts is used as input to an automatic routine that runs the code and compares the model to the observed data (calculating the rms of the differences). The "amoeba" routine performs multidimensional minimization of the rms, using the downhill simplex method of Nelder and Mead (1965). Local minima can be avoided by starting the process in different places in the parameter space. The routine also allows "weights" for different parts of the spectrum. The weights were varied between 1 and 0. The weights are taken into account when the rms is computed allowing us to control to which segment of the spectrum the fit should be tuned up. This tactic allows an extensive exploration of the parameter space, producing thousands of models. We find that when equal weight is given to the entire wavelength range the overall fit is poorer. Consequently, in the automatic procedure to model Quaoar, we chose to give all weight to the spectral part of the data, as the amount of information per segment of spectrum is higher than in the photometric bands.

3.3.3. Best model

Our best model consists of an intimate mixture of crystalline and amorphous H_2O, CH_4, N_2, and C_2H_6 ice with triton and titan tholin. Both crystalline H_2O and CH_4 ice are contaminated molecularly by triton and titan tholin as well. Details of the best fit (shown in Fig. 3) are listed in Table 4.

Table 4. Best fitting model, model without N_2, model with 10% N_2.

	Best Model	No N_2 model	10% N_2 model	Reference[e]
rms[a]	1.1×10^{-4}	1.8×10^{-4}	1.6×10^{-4}	–
Titan tholin [b]	0.12	0.09	0.11	(1)
Triton tholin [b]	0.06	0.05	0.04	(2)
Triton tholin [c]	0.03	0.05	0.04	(2)
H_2O amorph (40 K) [d]	0.18(1.3 μm)	0.29(1.5 μm)	0.22(1.8 μm)	(3)
Titan tholin [d]	0.13(11.2 μm)	0.14(11.8 μm)	0.13(12.0 μm)	(1)
H_2O cryst (40 K) [d]	0.18(14.6 μm)	0.24(11.0 μm)	0.23(11.4 μm)	(3)
C_2H_6 [d]	0.04(6.5 μm)	0.04(8.4 μm)	0.04(8.8 μm)	(4)
Triton tholin [d]	0.14(7.4 μm)	0.15(6.8 μm)	0.14(7.6 μm)	(2)
N_2 (36–60 K) [d]	0.20(16.1 mm)	0(16.0 mm)	0.1(15.8 mm)	(5)
CH_4 (30–35 K) [d]	0.13(9.4 μm)	0.14(7.1 μm)	0.16(8.4 μm)	(6), (7)

[a] rms error of each model when compared to the data.
[b] Material mixed as inclusions in CH_4 ice.
[c] Material mixed as inclusions in crystalline H_2O ice.
[d] Material mixed intimately, with grain size in parenthesis. Temperature listed after the name of the component.
[e] References. (1) Imanaka et al. (2005); (2) Khare et al. (1994); (3) Mastrapa & Sandford (2008); (4) Mastrapa (private comm); (5) Green et al. (1991); (6) Grundy et al. (2002); (7) Hudgins et al. (1993).
N.B.: All models were computed with a porosity of 0.1.

Fitting the overall shape of the albedo distribution on Quaoar turned out to be a challenging enterprise, mostly due to the overall fairly high albedo. While its visual albedo is only intermediate, Quaoar's steep red slope makes its near-IR and IRAC albedo levels high, comparable to that of Sedna. The relative heights of the two *Spitzer* bands complicate the problem even more.

Using a mix of crystalline H_2O and CH_4 ices with reddening materials yields a satisfactory fit up to 2.5 μm, but causes the model to be too dark at the wavelength of the *Spitzer* IRAC bands by about 40%. The low computed albedo at the *Spitzer* wavelengths is due to the relatively large amount of crystalline H_2O ice present in the mixture. H_2O ice reflectance, as shown in Fig. 2, is low at those wavelengths. The other materials, triton and titan tholin, as well as N_2 and CH_4 ice, are brighter, but not enough to completely counterbalance the effect of H_2O ice. Furthermore, CH_4 makes the first IRAC band lower than the second in contrast with the observations. Several attempts at raising the albedo in this region using a variety of materials have resulted in poor fits for the shorter wavelength data.

In our quest to find a material that reflects very efficiently at the *Spitzer* wavelengths we experimented with amorphous H_2O – brighter than crystalline H_2O ice in this region – in extremely small grains ($1\ \mu m < d \ll \lambda$): the fit is shown in Fig. 3 as the solid line and is our best fitting model. The broken line shows the same fit calculated with no amorphous H_2O ice as a comparison. It is evident that the amorphous H_2O ice increases the albedo at the wavelengths of the second *Spitzer* band improving the fit by about 20% at 4.5 μm. The grain size of the amorphous H_2O ice in the best model shown in the figure is slightly larger than 1.0 μm. Unfortunately, a grain size $\ll\lambda$ is not physically acceptable for a component in an intimate mixture, as in this case the theory does not accommodate diffractive behavior of the tiny particles. However, the result shown in Fig. 3 confirms the need for a very bright material. Broadening our search, we find that CO, like amorphous H_2O in tiny grains, can also be used as a placeholder as it has a high reflectivity across the observed wavelength range. When substituted in the model CO yields as good a fit as amorphous H_2O in tiny grains. The CO fundamental at 4.68 μm falls within the second IRAC band, but is so narrow that its overall effect on that band is small. The overtone at 2.35 μm is also narrow and falls in the middle of the complex bands of CH_4, so it is difficult to discern in the current data. CO has been detected on Pluto and Triton, and is a plausible component of Quaoar. Nevertheless, when CO is included in the model in place of amorphous H_2O the fit does not improve significantly, leading us to conclude that CO, even though a possible component, is not the final solution to the problem of finding the ingredient that has a high albedo at the IRAC wavelengths.

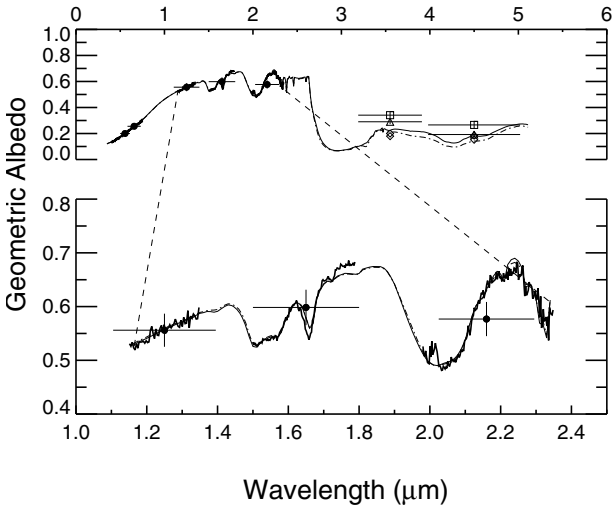

Fig. 3. Best fitting model (solid line) compared to a model computed with the same components except amorphous H_2O (broken line). Open diamonds show the model convolved to the Spitzer filter response functions. Open triangles mark the first *Spitzer* exposure, open squares indicate the position of the second. The model shows how amorphous H_2O increases the albedo in the *Spitzer* wavelength region. The observations were scaled to Stansberry et al. (2008) visual geometric albedo.

A scenario that should be considered is where the mixture of amorphous H_2O and other components is no longer a coarse-particle, intimate mixture. If the surface of Quaoar were covered with grains of crystalline H_2O ice mixed coarsely with CH_4, N_2, ethane ice and organic materials, and these grains were in turn covered with a very thin ($\ll\lambda$) layer of amorphous

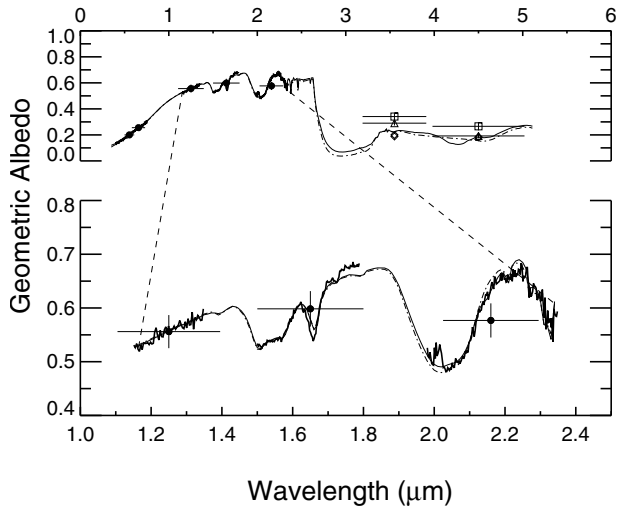

Fig. 4. A comparison of models with different amounts of N_2 in their composition. The solid thin line shows the best model comprising 20% N_2, the broken line shows the same model computed with no N_2. Open diamonds show the model convolved to the Spitzer filter response functions. Open triangles mark the first *Spitzer* exposure, open squares indicate the position of the second.

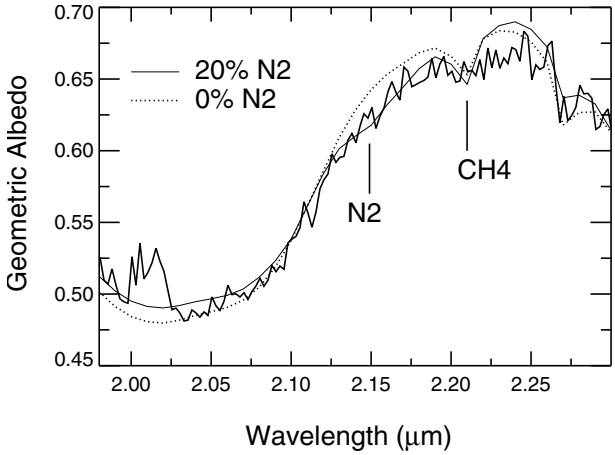

Fig. 5. Best fit (solid line) and fit without N_2. The fit at 2.149 μm marked with N_2 is moderately improved by the presence of 20% N_2 ice in the solid line model.

H_2O ice, this layer would effectively change the absorption and refractive properties of the underlying particles, and possibly yield a more reflective material (Shkuratov 1999; Starukhina & Shkuratov 1996). More calculations will be necessary to test this hypothesis.

Even with fine-grained amorphous H_2O, the model runs well below the measured albedo at 3.6 μm. Since we know from the rotation lightcurve that the first of the *Spitzer* IRAC exposures overlaps the ground data (only ~30° of separation in longitude) we can rule out the possibility of different terrains being sampled. Therefore, we are left with two possibilities for explaining this poor fit. The first lies with the optical constants that can have significant uncertainty, particularly in regions of increased transparency, where they are highly sensitive to the choice of baseline (e.g., Mastrapa et al. 2008). The ~3.4–3.8 μm is a relatively transparent region in H_2O ice: a large error associated with the optical constants in this region is expected and could be the culprit of the problem. Another possible explanation for the misfit at 3.6 μm is that there is still some component of the surface composition that we are missing.

We have included N_2 in our Quaoar model, a component that has not been detected on Quaoar before. N_2 ice contributes to the model in two ways: it improves the fit at 2.149 μm (Fig. 5) and it contributes to increasing the level of the albedo in the first *Spitzer* band at 3.6 μm (Fig. 4). In fact, when the amount of N_2 increases amorphous H_2O in small grains, the very bright component of the mixture, decreases to compensate, as shown in Table 4. Because the bands of N_2 ice are intrinsically weak, this material could be present in relatively large amounts (although less than on Triton and Pluto) and escape direct spectroscopic detection. However, from fitting the shape of the right wing of the 2 μm H_2O feature (Fig. 5) we find that a model including 20% N_2 (using hexagonal β-phase optical constants) yields a good fit, and therefore suggests that N_2 may be a significant component on Quaoar, although its spectral absorption band is not fully resolved.

Table 4 compares the best model (incorporating 20% N_2), to a model with 10% and no N_2 respectively to show how changing the amount of N_2 affects the other components. The first row shows the rms error of each model when compared to the data. The following two rows show the amount of the materials specified mixed as inclusions in CH_4, the third line the amount mixed as inclusions in crystalline H_2O ice. Their grain size is not listed as in this kind of mixture it is assumed to be $\ll\lambda$. The remaining materials listed in the table, with grain sizes in parenthesis, are mixed intimately. The temperatures of H_2O (amorphous and crystalline), CH_4 and N_2 ices are also listed after the name of the component.

It is difficult to assign an error estimate to the models as many of the parameters that enter in the calculation are not very well known and we do not have any evaluation of their uncertainty or, as in the case of the optical constans, the error can be extremely large and misleading. While the quality of fit of the preferred models is in fact sensitive to these parameters, once they have been selected the models are quite sensitive to the choice of abundance, grain size and mixing geometry of the components. In fact, when looking at Table 4, it is possible to calibrate the uncertainty of each component abundance and grain size in the models: while the amount of N_2 varies by as much as 20% the remaining components have to compensate. As already noted it is the H_2O in small grains that absorbs most of the change (by 11%), probably because of its lack of strong features that would otherwise constrain its abundance. The second component to change significantly (by 6%) is crystalline H_2O ice, compensating the larger amount by choosing a smaller grain size and allowing an equally good fit of the 1.5 and 2 μm bands. The remaining components vary by 1% at the most, indicating that the solution is fairly stable (as indicated also by the nearly constant rms among the different fits) and giving us a rough estimate of their error.

Following up on previous work suggesting that C_2H_6 and NH_4OH might be present on the surface of Quaoar (Schaller & Brown 2007b; and Jewitt & Luu 2004) we experimented introducing each among the main components in our best fitting model. Optical constants for NH_4OH (3% concentration of NH_3, 80 K temperature) were provided by Roush and were the same used by Bauer et al. (2002) in their study of Miranda's surface composition. NH_4OH has two bands in the IR part of the spectrum: at 2.0 and 2.2 μm. While the 2.0 μm band overlaps with H_2O ice, the second NH_4OH band overlaps with one of the CH_4 bands at 2.2 μm. Other bands confirm the presence of CH_4, preventing us from validating the NH_4OH detection. As far as C_2H_6 is concerned, a small amount of this component improves our

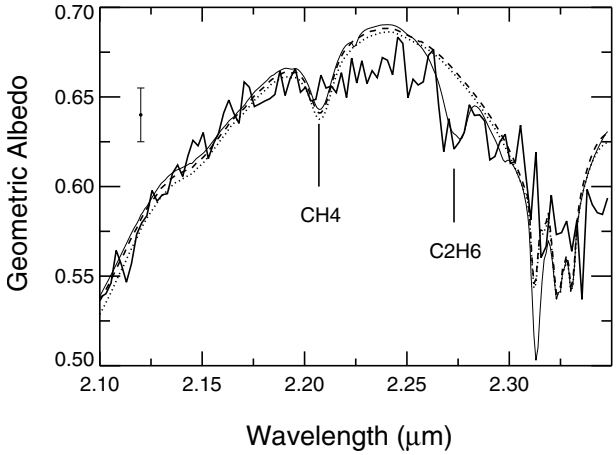

Fig. 6. Detail of the best fit (solid line), a fit without C_2H_6 (dashed), and a fit with NH_4OH in place of C_2H_6 (dotted). There is some evidence for C_2H_6 as shown by the fit to the 2.275 μm band. NH_4OH on the other hand does not seem to contribute significantly (at this low concentration).

best fit to the small absorption at ≃2.27 μm as shown in Fig. 6. The feature is hardly a detection as it is weak and close to the edge of the spectral data, however it is well matched by the synthetic spectrum. C_2H_6 has another, stronger band at ≃2.32 μm which falls very close to the edge of the spectrum where the noise level of the data is higher. When looking closely at this region of the spectrum the overall level of the absorption centered at ≃2.325 μm appears to be offset higher than the model. This could indicate a slight overestimate of the CH_4 abundance in the model. However, concerning C_2H_6, the pattern of the individual features in the ≃2.325 μm observed band shows the first of the three components at ≃2.318 μm, even though affected by a noise spike, to be indeed the strongest, as expected in the presence of C_2H_6. Based on this subtle, but supporting evidence, we confirm Schaller & Brown's (2007b) original suggestion until better spectral data for this wavelength region becomes available.

The best fit and its variations were all computed giving higher weight to the $\lambda < 2.5$ μm region and therefore forcing the program to converge to a good fit in the part of the spectrum where bands as well as albedo height both contributed to constrain the solution. When this constraint was relaxed the relative amounts of the components changed by a few percents to accommodate the requirement of a brighter than otherwise predicted IRAC albedo. The overall poorer fit still maintained the same components, confirming the need for the fairly large number of materials that constitute our best model.

3.4. H_2O ice temperature determination

Grundy & Schmitt (1998) showed that one of the most striking changes in the behavior of the crystalline H_2O ice spectrum with temperature is the wavelength shift at 1.65 μm. The shift is accompanied by temperature sensitive changes in the relative strength of the 1.65-μm band with respect to the adjacent H_2O band absorption maximum at 1.50 μm. We apply the same technique described by Merlin et al. (2007) in their analysis of 2003 EL61 to determine the central position of the band in the spectrum of Quaoar. We find the minimum of the band at 1.6578 ± 0.0010 μm corresponding to an estimated upper limit for the crystalline H_2O ice temperature of 30 K, where the error in wavelength includes both the uncertainty due to the calibration of the instrument and that of the measurement technique. The inferred temperature is lower than the Stefan Boltzmann value (40 K for a V albedo of 20%) possibly highlighting a problem in the assumptions. Indeed, because of the coincidence in wavelength of the 1.65-μm H_2O band with a band of CH_4, a shift in the observed absorption band may be caused by the presence of CH_4, thus confusing the temperature effect in the H_2O band.

To test to what degree CH_4 contamination could be responsible for the shift in wavelength we calculate models with H_2O, CH_4, and C_2H_6 in proportions similar to the relative amounts present on Quaoar. We find that the shift in the band position as a function of composition is only a fraction of the measured shift. To further understand the nature of the shift in the observed 1.65 μm band we compute models using two sets of optical constants for H_2O ice at 40 K – Mastrapa & Sandford (2008) and Grundy & Schmitt (1998) respectively – for which we know that the crystalline ice is in both its cubic and hexagonal phase for the former and purely hexagonal for the latter. The shifts in wavelengths for the corresponding synthetic spectra brace the shift of the observations pointing to the fact that Quaoar's crystalline H_2O ice could be present in both cubic and hexagonal form. High resolution and high signal-to-noise spectral data in the Spitzer wavelength range might be required to obtain a firmer determination of Quaoar's surface composition and in turn the ability to discern to what degree the shift in wavelength is due to composition or to other factors related to its temperature and history.

4. Conclusions

We present high signal-to-noise and high spectral resolution VLT data in conjunction with *Spitzer* data for Quaoar, a Transneptunian (Kuiper Belt) object. The spectral data cover the visual to near-infrared range while the *Spitzer Space Telescope* IRAC data consist of two photometric bands at 3.6 and 4.5 μm. This extended wavelength range provides a large set of constraints when modeling the surface composition of this object, narrowing down the number of possible solutions.

The overall high albedo of Quaoar is already an indication of the expected importance of ices on the surface of this TNO. Indeed, we confirm that the overall albedo shape and albedo levels can be fit by a combination of CH_4 and H_2O ice (already detected by Schaller & Brown 2007b) mixed both molecularly and intimately with tholins. Traces of ethane (also predicted by Schaller & Brown 2007b) are also indicated by the model fits. In addition, model fits suggest that N_2 may be a significant component which, if verified, would make this TNO even more similar to Triton and Pluto. However, in contrast to Pluto and Triton which have spectra dominated by CH_4, Quaoar's spectrum is dominated by H_2O ice. The much reduced ability of Quaoar to retain very volatile species compared to Pluto and Triton (Schaller & Brown 2007a) could have led to a very different evolution with time of the surface volatiles, with the less volatile H_2O ice being much more apparent.

Our data and models do not confirm the presence of NH_4OH as a significant contributor to the observed spectrum. As already discussed by Schaller & Brown (2007b), this lessens the need to call for cryovolcanism to explain Quaoar's surface composition.

Our attempt at measuring the temperature of H_2O ice on the surface of Quaoar based on the 1.65 μm crystalline ice feature yields an estimate of 30 K. This lower than expected value highlights the difficulty to obtain a firm measurement due to the presence of CH_4 mixed with H_2O ice as well as to the possibility that crystalline ice might be present in both cubic and hexagonal

phase on the surface of this KBO. A firmer determination of the composition will be necessary to make a more precise determination of the temperature and history of Quaoar.

Even our best-fit spectral model underestimates the albedo at the *Spitzer* wavelengths where crystalline H_2O ice is instead very absorbing. We find that a highly reflective material is required to fit the *Spitzer* data. We experiment with CO, which only partially fulfills this demand and can be used only as a placeholder as none of its features have been detected in the observed wavelength range. As an alternative, amorphous H_2O in grains $\ll\lambda$ could also satisfy this need if the mixing was not between coarse particles as intimate mixtures assume, but as a very thin layer of amorphous H_2O ice on top of the coarse mixture of the other components. in this case, the amorphous ice could be the result of irradiation of crystalline ice and represent a process that is part of the constant cycle of transformation of H_2O ice on the surface of this (and some other) distant icy bodies (e.g. Mastrapa & Brown 2006). However, it remains to be seen if it would be compatible with the presence of the irradiated carbon-containing species that are advocated to account for the red color of Quaoar. Additional irradiation experiments on ices, particularly on ices with impurities, and spectral models that are appropriate for very fine grain sizes and thin coatings or layers will further test this scenario.

Acknowledgements. C.M.D.O. would like to thank Dr. Ted Roush for many helpful conversations as well as help in the everlasting search for optical constants and Dr. Ludmilla Kolokolova for advice with modeling codes. This work is based [in part] on observations made with the *Spitzer* Space Telescope, which is operated by the Jet Propulsion Laboratory, California Institute of Technology under a contract with NASA. Support for this work was provided by NASA through an award issued by JPL/Caltech (program 20769).

References

Alvarez-Candal, A., Fornasier, S., Barucci, M. A., et al. 2008, A&A, 487, 741
Bagnulo, S., Boehnhardt, H., Muinonen, K., et al. 2006, A&A, 450, 1239
Bagnulo, S., Belskaya, I., Muinonen, K., et al. 2008, A&A, 491, L33
Baratta, G. A., Domingo, M., Ferini, G., et al. 2003, Nucl. Instrum. Methods Phys. Res. B, 209, 283
Barucci, M. A., Boehnhardt, H., Dotto, E., et al. 2002, A&A, 392, 335
Bauer, J. M., Roush, T. L., Geballe, T. R., et al. 2002, Icarus, 158, 178
Brown, M. E., & Suer, T.-A. 2007, IAU Circ., 8812, 1
Brown, M. E., & Trujillo, C. A. 2004, AJ, 127, 2413
Cook, J. C., Desch, S. J., & Roush, T. L. 2007, BAAS, 38, 510
Cruikshank, D. P., Imanaka, H., & Dalle Ore, C. M. 2005, Adv. Space Res., 36, 178
Delsanti, A. C., Hainaut, O., Jourdeuil, E., et al. 2004, A&A, 417, 1145
DeMeo, F. E., Fornasier, S., Barucci, M. A., et al. 2009, A&A, 493, 283
Fazio, G. G., Hora, J. L., Allen, L. E., et al. 2004, ApJS, 154, 10
Fornasier, S., Doressoundiram, A., Tozzi, G. P., et al. 2004, A&A, 421, 353
Green, J. R., Brown, R. H., Cruikshank, D. P., et al. 1991, BAAS, 23, 1208
Grundy, W. M., & Schmitt, B. 1998, J. Geophys. Res., 103, 25809
Grundy, W. M., Schmitt, B., & Quirico, E. 2002, Icarus, 155, 486
Guilbert, A., Alvarez-Candal, A., Merlin, F., et al. 2009, Icarus, 201, 272
Hapke, B. 1981, J. Geophys. Res., 86, 3039
Hudgins, D. M., Sandford, S. A., Allamandola, L. J., et al. 1993, ApJS, 86, 713
Imanaka, H., Khare, B. N., McKay, C. P., et al. 2005, BAAS, 37, 772
Jewitt, D. C., & Luu, J. 2004, Nature, 432, 731
Khare, B. N., Sagan, C., Heinrich, M., et al. 1994, BAAS, 26, 1176
Marchi, S., Lazzarin, M., Magrin, S., et al. 2003, A&A, 408, L17
Mastrapa, R. M. E., Bernstein, M. P., Sandford, S. A., et al. 2008, Icarus, 197, 307
Mastrapa, R. M. E., & Brown, R. H. 2006, Icarus, 183, 207
Mastrapa, R. M. E., & Sandford, S. A. 2008, AAS/Division for Planetary Sciences Meeting Abstracts, 40, #54.03
Merlin, F., Guilbert, A., Dumas, C., et al. 2007, A&A, 466, 1185
Moore, M. H., & Hudson, R. L. 2003, Icarus, 161, 486
Nelder, J., & Mead, R. 1965, Computer Journal, 7, 308
Olkin, C. B., Young, E. F., Young, L. A., et al. 2007, AJ, 133, 420
Ortiz, J. L., Gutiérrez, P. J., Sota, A., et al. 2003, A&A, 409, L13
Piscitelli, J. R., Cruikshank, D. P., & Bell, J. F. 1988, Icarus, 76, 118
Poulet, F., Cuzzi, J. N., Cruikshank, D. P., et al. 2003, Icarus, 160, 313
Protopapa, S., Boehnhardt, H., Herbst, T. M., et al. 2008, A&A, 490, 365
Rabinowitz, D. L., Schaefer, B. E., & Tourtellotte, S. W. 2007, AJ, 133, 26
Reach, W. T., Megeath, S. T., Cohen, M., et al. 2005, PASP, 117, 978
Schaller, E. L., & Brown, M. E. 2007a, ApJ, 659, L61
Schaller, E. L., & Brown, M. E. 2007b, ApJ, 670, L49
Shkuratov, Y., Starukhina, L., Hoffmann, H., et al. 1999, Icarus, 137, 235
Smith, E. V. P., & Gottlieb, D. M. 1974, Space Sci. Rev., 16, 771
Stansberry, J., Grundy, W., Brown, M., et al. 2008, in Solar System Beyond Neptune, ed. M. A. Barucci et al. (Univ. of Arizona Press), 161
Starukhina, L. V., & Shkuratov, Y. G. 1996, Solar System Research, 30, 299
Werner, M. W., Roellig, T. L., Low, F. J., et al. 2004, ApJS, 154, 1